JCI insight

RESEARCH ARTICLE

Cardiovascular response to small-molecule APJ activation

Brandon Ason,[1] Yinhong Chen,[1] Qi Guo,[1] Kimberly M. Hoagland,[2] Ray W. Chui,[2] Mark Fielden,[2] Weston Sutherland,[2] Rhonda Chen,[1] Ying Zhang,[1] Shirley Mihardja,[1] Xiaochuan Ma,[3] Xun Li,[3] Yaping Sun,[3] Dongming Liu,[1] Khanh Nguyen,[1] Jinghong Wang,[1] Ning Li,[1] Sridharan Rajamani,[1] Yusheng Qu,[2] BaoXi Gao,[2] Andrea Boden,[2] Vishnu Chintalgattu,[1] Jim R. Turk,[2] Joyce Chan,[1] Liaoyuan A. Hu,[3] Paul Dransfield,[4] Jonathan Houze,[4] Jingman Wong,[1] Ji Ma,[1] Vatee Pattaropong,[4] Murielle M. Véniant,[2] Hugo M. Vargas,[2] Gayathri Swaminath,[1] and Aarif Y. Khakoo[1]

[1]Amgen Research, South San Francisco, California, USA. [2]Amgen Research, Thousand Oaks, California, USA. [3]Amgen Research, Amgen Asia R&D Center, Shanghai, China. [4]Amgen Research, Cambridge, Massachusetts, USA.

Heart failure (HF) remains a grievous illness with poor prognosis even with optimal care. The apelin receptor (APJ) counteracts the pressor effect of angiotensin II, attenuates ischemic injury, and has the potential to be a novel target to treat HF. Intravenous administration of apelin improves cardiac function acutely in patients with HF. However, its short half-life restricts its use to infusion therapy. To identify a longer acting APJ agonist, we conducted a medicinal chemistry campaign, leading to the discovery of potent small-molecule APJ agonists with comparable activity to apelin by mimicking the C-terminal portion of apelin-13. Acute infusion increased systolic function and reduced systemic vascular resistance in 2 rat models of impaired cardiac function. Similar results were obtained in an anesthetized but not a conscious canine HF model. Chronic oral dosing in a rat myocardial infarction model reduced myocardial collagen content and improved diastolic function to a similar extent as losartan, a RAS antagonist standard-of-care therapy, but lacked additivity with coadministration. Collectively, this work demonstrates the feasibility of developing clinical, viable, potent small-molecule agonists that mimic the endogenous APJ ligand with more favorable drug-like properties and highlights potential limitations for APJ agonism for this indication.

Introduction

Heart failure (HF) is a grievous disease caused by diverse forms of cardiac injury and carries a 4-year mortality rate of 60% in the developed world (1, 2). An index event, such as an acute myocardial infarction (MI), typically leads to changes at multiple levels of the cardiac neuraxis. Although this response may be beneficial in the short term, chronic activation of these stress signals leads to maladaptive cardiac structural remodeling and fuels continued disease progression. Current treatments are focused on antagonizing neurohormonal and hemodynamic stress (3–5). Despite current guideline-directed medical care, there are more than 500,000 new HF cases per year, with more people in the United States dying from heart disease or associated disorders than from all forms of cancer combined (6, 7). Given these grim statistics, additional therapies are needed to improve patient outcomes.

Apelin receptor (APJ, APLNR) is a G protein–coupled receptor that shares homology with the angiotensin II type 1 receptor (AT1R) (8). APJ is expressed in endothelial and smooth muscle cells of the coronary and pulmonary vasculature as well as in the myocardium (9–12). APJ expression is induced by hypoxia, hyperreninemia, and hypoosmolality, all biological derangements associated with HF (13–17). The apelin-APJ axis negatively regulates angiotensin II–AT1R action on vascular tone and fluid homeostasis and has been proposed to function as part of a well-preserved evolutionary response to biological stress (18–24). Nonclinical and clinical studies show that APJ may be initially elevated in association with myocardial ischemia or HF but decreased in advanced left ventricular (LV) hypertrophy (9, 11, 23, 25–29).

Apelin and ELABELA are natural ligands of APJ, which are expressed as prepropeptides that are processed into biologically active isoforms (30, 31). ELABELA is expressed as a 54–amino acid precursor that is processed into 32–, 22–, and 11–amino acid active isoforms, while apelin is expressed as a 77–amino acid

Authorship note: BA, YC, QG, and KMH contributed equally to this work.

Conflict of interest: All authors are or were employed by Amgen.

Submitted: August 21, 2019
Accepted: March 18, 2020
Published: April 23, 2020.

Reference information: *JCI Insight*. 2020;5(8):e132898. https://doi.org/10.1172/jci.insight.132898.

precursor that is processed into 36–, 17–, 13–, and 12–amino acid active isoforms (12, 32–34). All exhibit a short half-life that is thought to enable a rapid and transient response to homeostatic perturbations. Administration of both apelin and ELABELA improve cardiac function in nonclinical models (35–40). Additionally, the most potent biologically active form of apelin, pyr-apelin-13, improves cardiac function acutely in healthy volunteers as well as in patients with HF, suggesting that stimulation of the apelin/APJ axis could be beneficial in this disease setting (41, 42). However, the short half-life of apelin peptides greatly limits their therapeutic utility for patients with chronic HF. Here, we set out to develop potent and safe small-molecule activators of APJ that have pharmacokinetic properties suitable for chronic administration. Furthermore, we sought to test the efficacy of these molecules in nonclinical models of cardiac disease to support their development for patients with HF.

Results

APJ small-molecule agonists AM-8123 and AMG 986 activate the APJ receptor in a manner similar to the endogenous ligands. A medicinal chemistry–based drug discovery approach was used to identify AM-8123 and AMG 986. In brief, a high-throughput screening campaign identified hits that were triaged through a cAMP assay that measured intracellular cAMP levels induced by APJ activation and a human GTPγS binding assay that measured Gα protein–stimulated receptor activation. Screening hits were subsequently tested against AT1 and β_2-adrenergic receptor, as antitargets to confirm selectivity for APJ.

The high-throughput screen resulted in 6 screening hits (3 of which were fragments with $EC_{50} > 5$ μM). From the 3 remaining hits, 6-chloro-2-(((4-(2-methoxyphenyl)-5-(thiophen-2-yl)-4H-1,2,4-triazol-3-yl)thio)methyl)imidazo[1,2-a]pyridine was selected as a validated hit as a series of close analogs exhibited tractable structure-activity relationship (SAR). A SAR campaign was subsequently undertaken, resulting in the discovery of several potent small-molecule agonists of APJ, which will be the subject of upcoming journal articles, of which AM-8123, (1S,2S)-N-(4-(2,6-dimethoxyphenyl)-5-(5-methylpyridin-3-yl)-4H-1,2,4-triazol-3-yl)-1-isopropoxy-1-(5-methylpyrimidin-2-yl)propane-2-sulfonamide, and the related compound AMG 986, (2S,3R)-N-(4-(2,6-dimethoxyphenyl)-5-(5-methyl-3-pyridinyl)-4H-1,2,4-triazol-3-yl)-3-(5-methyl-2-pyrimidinyl)-2-butanesulfonamide, were selected for further study due to exhibiting in vitro and in vivo properties that Amgen believes desirable in a clinical compound. These molecules were prepared as described (US patent WO2016187308A1, Triazole agonists of the APJ receptor) (43).

Both AM-8123 and AMG 986 inhibited forskolin-stimulated cAMP production and promoted Gα protein activation (Figure 1, A–C). Both molecules were slightly less potent in comparison with the endogenous ligand, pyr-apelin-13, in the cAMP assay (log EC_{50} AM-8123: –9.44 ± 0.04, AMG 986: –9.64 ± 0.03, pyr-apelin-13: –9.93 ± 0.03), while they were more potent relative to pyr-apelin-13 in the GTPγS assay (log EC_{50} AM-8123: –8.95 ± 0.05, AMG 986: –9.54 ± 0.03, pyr-apelin-13: –8.10 ± 0.05). The maximum level of activation for AM-8123 and AMG 986 were equal to (Figure 1B) or greater than pyr-apelin-13 (Figure 1C). Together, these data indicate that the small molecules are full APJ agonists that exhibit slight differences in potency relative to one another and may be more potent when compared with the endogenous ligand pyr-apelin-13.

APJ activation results in β-arrestin recruitment and receptor internalization (44, 45). We compared the potency of AM-8123, AMG 986, and pyr-apelin-13 to recruit β-arrestin using the PathHunter arrestin assay. In this assay, both AM-8123 and AMG 986 exhibited a modest increase in potency relative to pyr-apelin-13 (log EC_{50} AM-8123: –9.45 ± 0.08, AMG 986: –9.61 ± 0.13, pyr-apelin-13: –8.96 ± 0.03, Figure 1D). APJ internalization following receptor activation was additionally assessed by the PathHunter internalization assay. In U2OS cells that overexpress hAPJ, both AM-8123 and AMG 986 also resulted in receptor internalization with greater potency relative to pyr-apelin-13 (log EC_{50} AM-8123: –9.4 ± 0.03, AMG 986: –9.59 ± 0.03, pyr-apelin-13: –7.80 ± 0.04; Figure 1E).

Using an alternative method, we additionally monitored AM-8123–induced β-arrestin recruitment and receptor internalization using confocal microscopy. U2OS cells stably expressing C-terminal GFP-tagged β-arrestin were transiently transfected with hemagglutinin-tagged (HA-tagged) receptors using the BacMam system. β-arrestin and APJ receptor were visualized by GFP (green) and Alexa Fluor 594–conjugated anti-HA antibody (red), respectively (Supplemental Figure 1; supplemental material available online with this article; https://doi.org/10.1172/jci.insight.132898DS1). In APJ-expressing cells, treatment with both 100 nM AM-8123 and 1 μM apelin-13 caused a rapid β-arrestin translocation from cytoplasm to plasma membrane. The APJ/β-arrestin complexes formed and then internalized into cytosol to form intracellular vesicles within 30 minutes (Supplemental Figure 1). Collectively, these data suggest that both small molecules are functionally

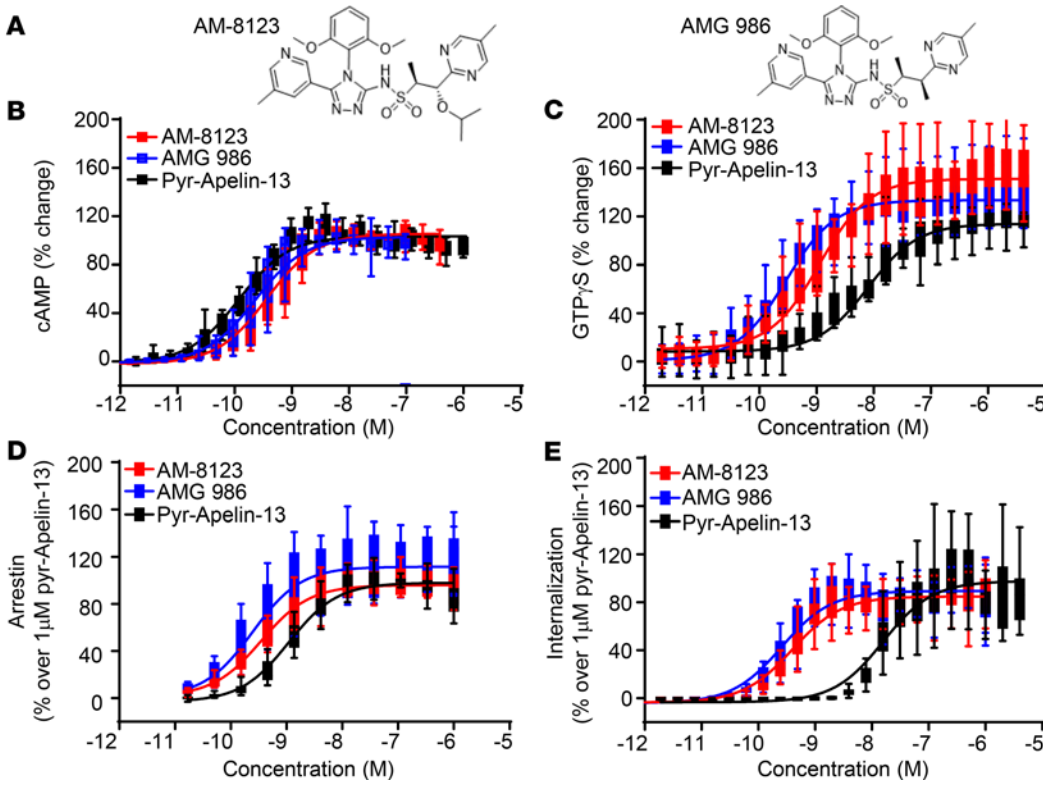

Figure 1. APJ receptor activation with small-molecule agonists and endogenous ligand. (**A**) The chemical structure of AM-8123 and AMG 986. The APJ small-molecule agonists AM-8123 (shown in red) and AMG 986 (shown in blue) and the endogenous ligand pyr-apelin-13 (shown in black) alter (**B**) cAMP levels (8, 16, and 10 individual experiments for each concentration of AM-8123, AMG 986, and pyr-apelin-13, respectively) and promote binding of nonhydrolyzable (**C**) GTPγS (14, 24, and 16 individual experiments for each concentration of AM-8123, AMG 986, and pyr-apelin-13, respectively) in human APJ–overexpressing (hAPJ-overexpressing) cells. Both AM-8123 and AMG 986 activation of hAPJ led to (**D**) β-arrestin recruitment (8, 8, and 24 individual experiments for each concentration of AM-8123, AMG 986, and pyr-apelin-13, respectively) and (**E**) receptor internalization (24 individual experiments per group) in a dose-dependent manner. Data shown as a box-and-whisker plot with a line indicating the median, the box representing the 25th–75th interquartile range, and the whiskers, calculated with Tukey's method.

equivalent. They are full agonists that activate APJ with potentially greater potency relative to the endogenous ligand and are capable of triggering β-arrestin recruitment and receptor internalization.

Molecular modeling of WT APJ in complex with either apelin-13 or AM-8123. Molecular modeling was subsequently used to determine whether the small-molecule agonists share the same binding site as the endogenous ligand apelin-13. The initial model of APJ (residues 19–330) in complex with apelin-13 was built via homology modeling in Discovery Studio (Dassault Systèmes BIOVIA, Discovery Studio Modeling Environment, Release 2017), with the previously published APJ-AMG3054 structure (Protein Data Bank [PDB] ID 5VBL) as the template (46). The third intracellular loop (ICL3) region was optimized with Prime Refine Loops in Schrödinger (Schrödinger Release 2017-3: Prime, Schrödinger, LLC). The models of APJ in complex with apelin-13 or AM-8123 were subsequently used to compare their binding modes (Figure 2, regions 1–4). The results suggest that AM-8123 can mimic the C-terminal part of apelin-13 through the following interactions: (region 1) the methylpyrimidine ring inserts into the subpocket composed of K268$^{6.55}$, Y271$^{6.58}$, M272$^{6.59}$, M288$^{7.32}$, and F291$^{7.35}$, as the side chain of apelin-13 Met11; (region 2) the sulfonamide and triazole group interacts with R168$^{4.64}$ and K268$^{6.55}$, mimicking the carbonyl group of apelin-13 Met11 and the carboxyl group of Phe13; and (region 3) the dimethoxyphenyl group mimics the phenyl ring of apelin-13 Phe13, which interacts with Y35$^{1.39}$, W85$^{2.60}$, Y88$^{2.63}$, F291$^{7.35}$, T295$^{7.39}$, and Y299$^{7.43}$. With all the above elements similar to apelin-13, AM-8123 can be considered an apelin-13 C-terminal mimetic ligand. Moreover, it has some unique elements, and the major one is its methylpyridine group (region 4) that inserts deeper into the orthosteric site than apelin-13, forming interactions with the subpocket composed of F78$^{2.53}$, I109$^{3.32}$, F110$^{3.33}$, M113$^{3.36}$, Y264$^{6.51}$, T295$^{7.39}$, and Y299$^{7.43}$. Taken together, these interactions may

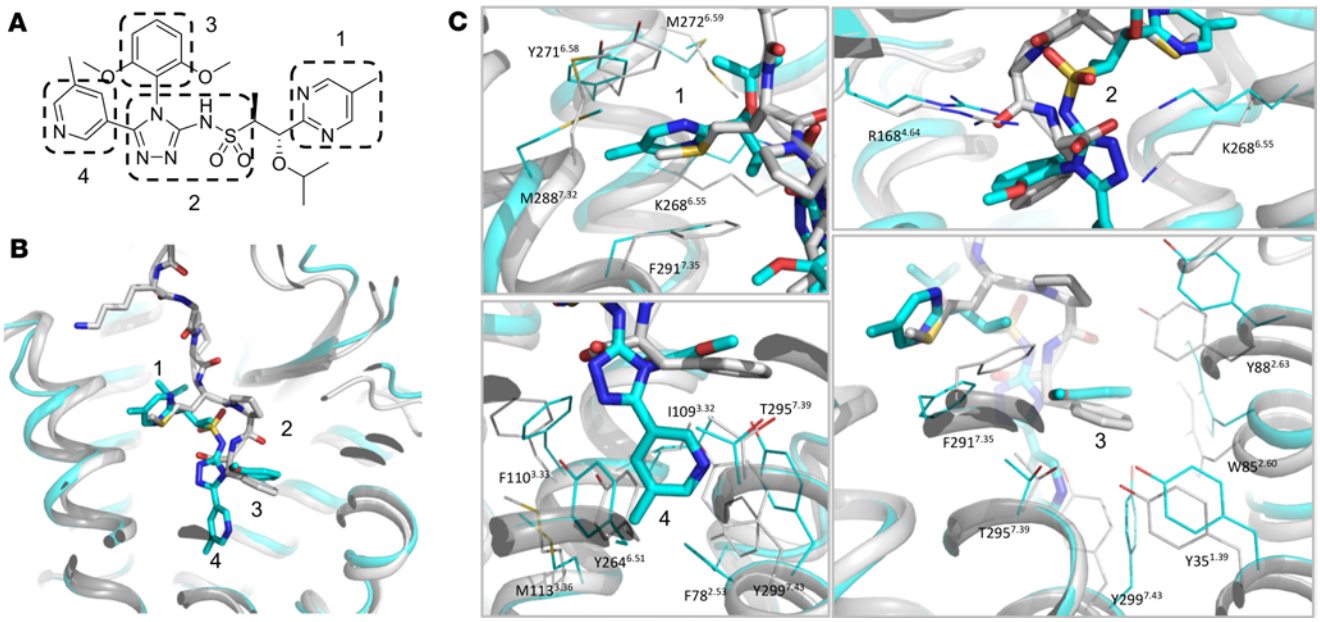

Figure 2. Molecular modeling overlay of WT APJ in complex with apelin-13 (in white) and AM-8123 (in cyan). (**A**) The chemical structure of AM-8123 and regions 1–4 involved in interactions with APJ. (**B**) The overview of binding modes of apelin-13 and AM-8123 at APJ orthosteric site with labeled regions 1–4. (**C**) Detailed interactions of regions 1–4. The protein is shown as cartoon, apelin-13 and AM-8123 are shown as sticks, and the residues are shown as lines.

explain why AM-8123 is a potent agonist of APJ even though it is smaller than the endogenous peptide ligand. Given the structural similarities between AM-8123 and AMG 986, we can infer that these interactions exist for both of these functionally equivalent molecules.

We next determined if mutations in APJ influence binding of the APJ small-molecule agonists by saturation binding of ^{3}H AM-8123. AM-8123 bound the native hAPJ receptor with low nanomolar affinity, consistent with the potency observed in the in vitro activity assays (Table 1). Several mutations (W85A, F110A, Y185A, K268A, Y271A, M288A, and F291A) impaired binding of AM-8123 (Table 1), indicating that interactions with transmembrane helices 2, 3, 6, and 7, as well as extracellular loop 2, which were predicted to interact with AM-8123 based on the molecular modeling, are important for proper formation of the small-molecule binding pocket.

AM-8123 and AMG 986 exhibit improved pharmacokinetic profile relative to pyr-apelin-13. To support chronic oral dosing of AM-8123 and AMG 986 in nonclinical studies and clinically, the pharmacokinetic properties of both were evaluated in rat and dog by both the IV (0.5 mg/kg) and oral (2 mg/kg) routes of administration (Table 2). Mean compartmental PK parameters indicated that Vss was low in dogs (0.33 and 0.94 L/kg for AM-8123 and AMG 986, respectively) and above total body water in rats (0.81 and 0.6 L/kg for AM-8123 and AMG 986, respectively). Clearance was low in dog and moderate in rat for both AM-8123 and AMG 986 following a single IV dose. The terminal half-life after IV dosing was 3.2 and 2.2 hours and 2.39 and 4.2 hours in rats and dogs for AM-8123 and AMG 986, respectively. Both AM-8123 and AMG 986 exhibited appreciably greater oral bioavailability in rats and dogs relative to pyr-apelin-13. The drug-like properties of AM-8123 and AMG 986 dramatically improved upon the short half-life of pyr-apelin-13 and were predicted to provide adequate exposures in humans with once-daily oral dosing.

Acute IV infusion of the APJ small-molecule agonist AMG 986 altered cardiac hemodynamics and increased cardiac reserve during dobutamine challenge in a rat model of impaired metabolic function. To assess the impact of APJ activation on cardiac function, AMG 986 was infused in ZSF1 obese rats, a model of diastolic dysfunction driven by abnormalities in metabolism, endothelial dysfunction, and hypertension. A 2-compartment model and PK parameters from an IV bolus study were used to select a dose that would result in a total plasma concentration within the low micromole range (V1 = 0.228511 L/kg, k10 = 3.400481, k12 = 0.770357, k21 = 1.719881). AMG 986 was infused at 1 mg/kg/min for 10 minutes, followed by a 5-minute coinfusion with dobutamine (12 μg/kg/min) to measure cardiac reserve (Figure 3A). Hemodynamic assessments were done invasively using a pressure-volume conductance

Table 1. Several APJ mutations impair binding to AM-8123

Residue	TM helix	K_D (nM)	Bmax	No. exps
WT	NA	4 ± 2	3600 ± 1400	10
Y35A	TM1	1 ± 1	1100 ± 600	6
W85A	TM2	Too weak to determine	Too weak to determine	4
F110A	TM3	42 ± 40	5900 ± 4200	5
M113A	TM3	8 ± 6	4400 ± 2800	9
R168A	ECL2	12 ± 8	5800 ± 3200	6
Y185A	ECL2	Too weak to determine	Too weak to determine	6
E198A	TM5	7 ± 3	2700 ± 900	5
K268A	TM6	Too weak to determine	Too weak to determine	6
Y271A	TM6	Too weak to determine	Too weak to determine	7
M288A	TM7	23 ± 8	4000 ± 1800	3
F291A	TM7	Too weak to determine	Too weak to determine	7
T295A	TM7	10 ± 11	3000 ± 1700	8

TM, transmembrane; Bmax, maximum specific binding; No. exps, number of experiments; ECL, extracellular loop.

catheter to give a direct and continuous measure of cardiac function. Acute administration of AMG 986 resulted in an unbound plasma exposure of 0.87 μM and a modest but significant increase in stroke volume (SV), ejection fraction (EF), and heart rate (HR) while mean arterial pressure (MAP) remained unchanged when compared with vehicle (Figure 3, B and C; and Supplemental Figure 2). Additionally, AMG 986 decreased the MAP/cardiac output (MAP/CO) ratio, which is used to approximate systemic vascular resistance (SVR), suggesting a decrease in cardiac afterload (Figure 3D). AMG 986 coinfusion with dobutamine led to a more robust increase in SV without significantly altering MAP or HR relative to dobutamine alone, providing evidence that AMG 986 enhanced cardiac reserve following dobutamine challenge in a metabolic model of diastolic dysfunction.

Acute IV infusion of the APJ small-molecule agonist AM-8123 improves cardiac function in a rat MI model. Because the small-molecule agonist primarily affected systolic function in ZSF1 obese rats, a model in which systolic function is largely preserved, we next assessed how APJ receptor activation improves systolic function in a rat model of acute post-MI systolic HF. In vivo cardiovascular hemodynamics were collected invasively 6–8 weeks post-MI from animals infused with AM-8123 using a pressure-volume conductance catheter. Animals were enrolled in the study if an infarct, induced by left anterior descending artery (LAD) ligation, resulted in an EF of no more than 45% as measured by echocardiography. Animals meeting these criteria were randomly assigned to one of the 5 dose groups (Supplemental Figure 3A). Acute infusion of AM-8123 decreased MAP/CO, suggesting a decrease in SVR or cardiac afterload (Supplemental Figure 3B). Additionally, AM-8123 infusion resulted in an increase in EF, SV, and *dP/dt* max at submicromolar unbound plasma concentrations with minimal change in HR, indicating that acute infusion of AM-8123 is associated with an improvement in several markers of cardiac function (Supplemental Figure 3, C–H). A transient drop in MAP (–12% and –17%) was observed 1 minute following the initial infusion for the high-dose groups (0.2 and 2 mg/kg) that returned to baseline for the 2 mg/kg group and continued to rise above baseline levels for the 0.2 mg/kg group (Supplemental Figure 3H). Collectively, these results are comparable with the hemodynamic profile observed following an acute infusion of the endogenous ligand, pyr-apelin-13, in this model (Supplemental Figure 4).

Chronic oral administration of the APJ small-molecule agonist AM-8123 reduces collagen burden and improves cardiac function in an MI rat model. To determine how the acute hemodynamic changes observed in the MI model translate to alterations in cardiac performance over longer periods of exposure, we next measured cardiovascular function during 8 weeks of twice-daily oral administration of AM-8123 with or without coadministration of losartan, a standard-of-care therapy for systolic HF. Lewis rats (2–3 months old) underwent permanent LAD ligation to generate MI-induced HF. Echocardiography was performed 1 week post-MI for baseline values and animal exclusion prior to treatment initiation. Animals with an EF of no more than 45% and a medium infarct 1 week post-MI were randomly assigned to 4 groups (vehicle, AM-8123, losartan, or AM-8123 + losartan). AM-8123 (100 mg/kg) and vehicle were administered

Table 2. AMG 986 and AM-8123 exhibit an improved PK profile

	CL (L/h/kg)		Vss (L/kg) (volume distribution steady state)		Terminal half-life (h)		%F (oral bioavailability)	
	Rat	Dog	Rat	Dog	Rat	Dog	Rat	Dog
Pyr-apelin-13	357	4.3	9.3	0.7	0.02	0.11	<1	<1
AMG 986	0.78	0.08	0.6	0.19	2.4	4.2	73	97
AM-8123	0.62	0.32	0.81	0.33	3.2	2.2	60	40

PK, pharmacokinetic; CL, clearance.

twice daily for 9 weeks. Losartan (0.5 g/L) was administered in drinking water, ad libitum. Echocardiography was performed at 4 and 8 weeks postinitiation of treatment for assessment of cardiovascular function. Invasive hemodynamic assessment of cardiac function was performed using a pressure-volume conductance catheter at study termination (9 weeks after treatment initiation, 10 weeks following LAD ligation surgeries) to complement the noninvasive echocardiographic endpoints (Figure 4A). Sustained levels of exposure were maintained for both AM-8123– and losartan-treated groups (Supplemental Figure 5). These treatments did not alter body weight over the course of the study (Supplemental Figure 6A). As expected, progression of the LV chamber dilation and deterioration of cardiac function occurred in MI-induced HF animals. Fractional shortening (FS) and EF were sharply reduced 1 week post-MI from normal levels (FS from ~22% reduced to ~16% and EF from ~60% reduced to ~40% at long axis-B mode) (Supplemental Figure 6, B and C).

Over the 2-month period, EF and FS declined while end-diastolic volume (EDV) and end-systolic volume (ESV) increased in vehicle-treated MI animals (Supplemental Figure 6, B–E). Chronic treatment with AM-8123 alone resulted in sustained improvement in systolic function, reflected by a significant increase in FS (Supplemental Figure 6B) and EF (Figure 4D and Supplemental Figure 6C). AM-8123 alone decreased both EDV and ESV as measured by echocardiography but not by the invasive pressure-volume conductance catheter at study termination (Supplemental Figures 6, D and E, and 7, A and B). These improvements occurred without a meaningful change in HR (Supplemental Figure 6F) or MAP (Supplemental Figure 7C) when compared to vehicle. The improvement in cardiovascular function observed for AM-8123 was comparable in magnitude to the level of improvement observed for losartan alone without the observed decrease in MAP that was associated with losartan treatment (Figure 4, Supplemental Figure 6, and Supplemental Figure 7), suggesting that AM-8123 can improve cardiac function in the absence of sustained changes in blood pressure. The combination of AM-8123 with losartan did not result in further increase in EF and FS compared to monotherapy but did result in a significant decrease in SVR, which trended lower for each monotherapy alone, only reaching significance when combined (Supplemental Figure 7D).

Inotropic agents such as dobutamine are known to induce cardiac hypertrophy (47, 48). However, no evidence of cardiac hypertrophy was observed following chronic administration of AM-8123 (Supplemental Figure 7E). In addition to assessment of cardiac hypertrophy by weight, histological analysis further confirmed no significant difference in total myocardial volume among the treated groups when compared to the vehicle (Supplemental Figure 7F). A significant reduction in collagen deposition was observed as measured by Picrosirius red in all 3 treatment groups when compared with vehicle control, suggesting an improvement in post-MI remodeling and attenuated expansion of the border zone (Figure 4, B and C). The reduction in collagen deposition was associated with a trend toward a reduction in collagen 1A1 and periostin gene mRNA expression for both the AM-8123– and losartan-treated groups (Supplemental Figure 8).

Additionally, chronic administration of AM-8123 and losartan, either alone or in combination, improved diastolic function as evidenced by a significant decrease in the isovolumetric relaxation constant (Supplemental Figure 6G) and the E/E′ ratio (Supplemental Figure 6H), both markers of myocardial stiffness. Both the relaxation constant tau (Supplemental Figure 7G) and LV filling pressure, end-diastolic pressure (Supplemental Figure 7H), trended lower following losartan treatment. The effect was more pronounced for the AM-8123 + losartan combination group, reaching significance for tau. This suggests that the reduction in collagen content improved myocardial compliance following sustained exposure to either AM-8123 or losartan.

The improvement in cardiac function by the APJ small-molecule agonist AM-8123 was associated with a significant increase in ERK phosphorylation and a trend toward increased AKT, endothelial NOS

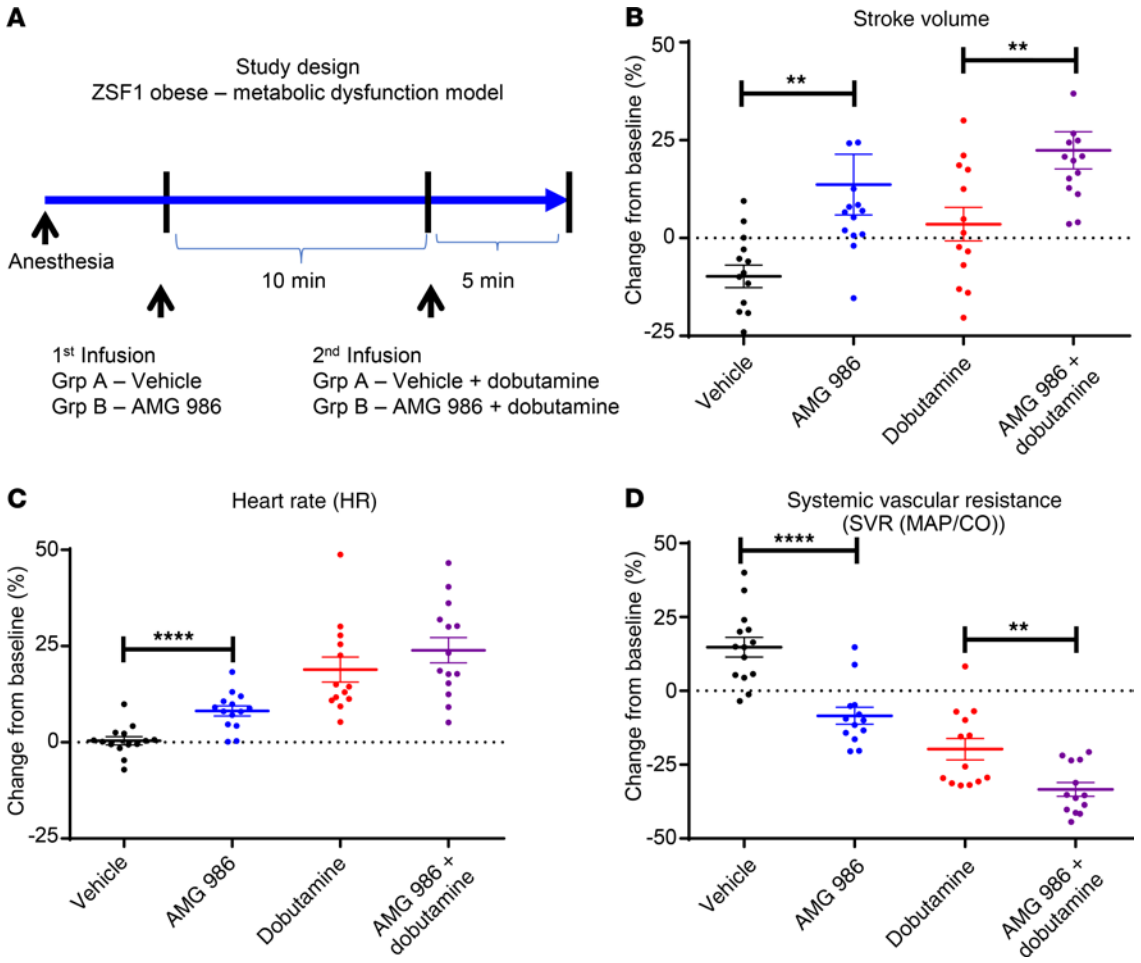

Figure 3. Acute infusion of the APJ small-molecule agonist AMG 986 increases cardiac reserve during dobutamine challenge in a rat model of impaired metabolic function. (**A**) ZSF1 obese rats (19 weeks old) were randomized into 2 groups based on a measure of diastolic function (E/E′: 21 ± 4) and body weight (vehicle: 524 ± 21 g, AMG 986: 532 ± 25 g). AMG 986 (1 mg/kg/min) or vehicle was infused for 10 minutes following catheterization and baseline stabilization. Dobutamine (12 μg/kg/min) was coadministered for an additional 5 minutes to measure cardiac reserve capacity. The effect of AMG 986 infusion ± dobutamine on (**B**) SV, (**C**) HR, and (**D**) SVR relative to vehicle is shown. Data shown as individual animals (circles) together with the group mean (bars) ± SEM. *n* = 13–14 animals per group. Data analyses performed blinded. Significance measured by a 2-tailed unpaired *t* test (***P* < 0.01; *****P* < 0.0001).

(eNOS), and AMPK phosphorylation in LV cardiac tissue following chronic administration (Figure 5, A and B; and Supplemental Figure 9). Both AM-8123 and pyr-apelin-13 resulted in ERK phosphorylation in HUVECs grown under hypoxic conditions, suggesting that endothelial cells may play a role in the beneficial effects of APJ activation on cardiac function following injury (Figure 6A). Additionally, both AM-8123 and pyr-apelin-13 mediated ERK and AKT phosphorylation in cells overexpressing hAPJ (Figure 6, B and C). As observed in the GTPγS binding, β-arrestin recruitment, and internalization in vitro assays, AM-8123 is a more potent mediator of both ERK and AKT phosphorylation relative to pyr-apelin-13 (ERK log EC_{50} –9.30 ± 0.09 and –8.06 ± 0.15, AKT log EC_{50} –8.98 ± 0.07 and –7.67 ± 0.05, respectively).

Acute IV administration of AM-8123 improves cardiovascular function in an anesthetized, tachypaced canine HF model. To determine whether the improvements in cardiac function observed in the rat models translate to a large-animal model, we next evaluated AM-8123 in both conscious and anesthetized tachypacing-induced HF beagles. In vivo cardiovascular endpoints were measured by telemetry implants collecting electrocardiograms (ECGs), systemic arterial pressure, LV pressure, aortic flow, and LV dimensional data. Each animal was subjected to 4 interventions in a randomized manner, with each separated by at least 1 week, to allow recovery: (a) vehicle treatment under isoflurane anesthesia, (b) AM-8123 under isoflurane, (c) vehicle treatment in conscious state, and (d) AM-8123 in conscious state (Figure 7A).

IV administration of AM-8123 at 0.035, 0.09, 0.9, and 9 mg/kg evoked a dose-dependent increase in unbound AM-8123 in plasma (Figure 7B) that was associated with a dose-dependent increase in cardiac

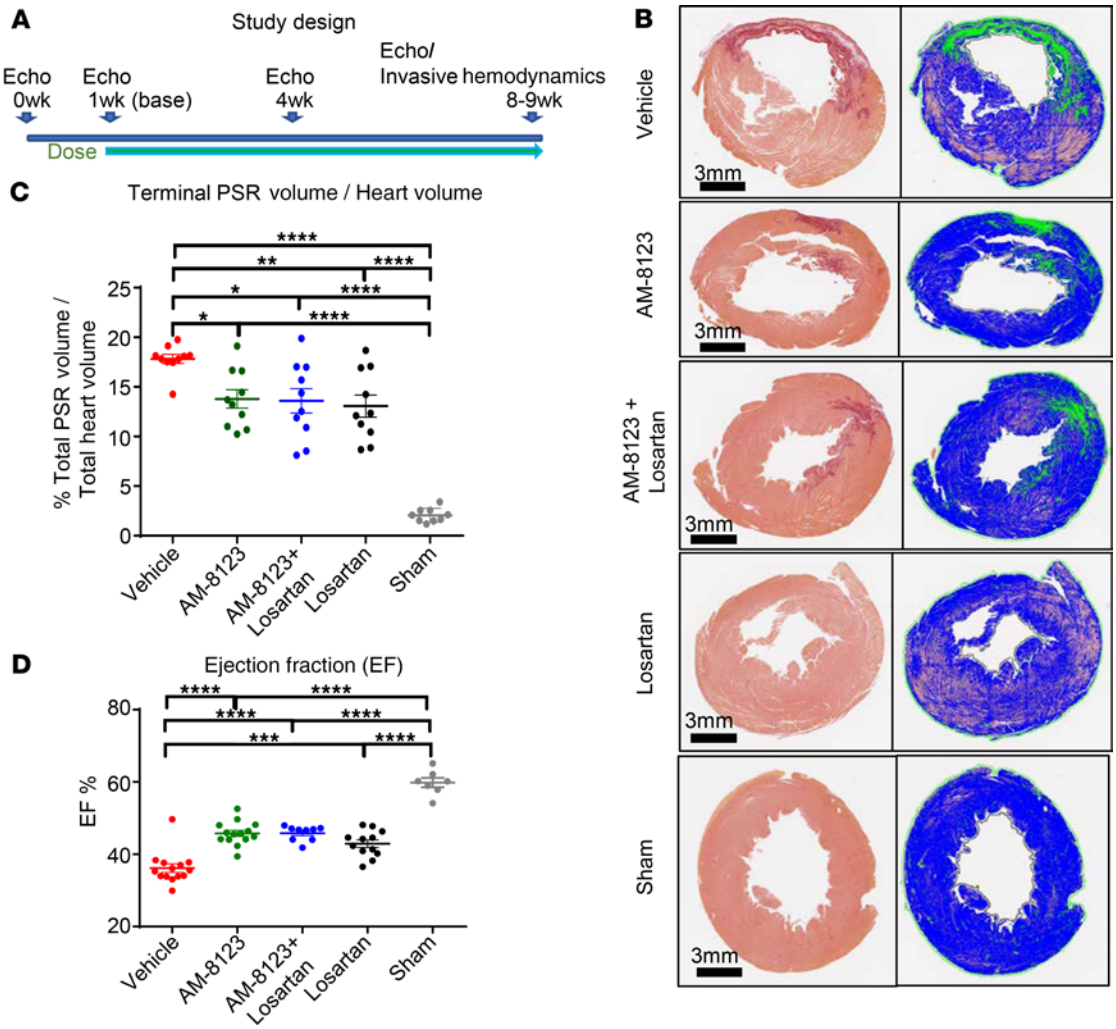

Figure 4. Chronic administration of AM-8123 increases EF and reduces collagen burden in an LAD ligation–induced MI rat model. (**A**) Rats were treated with vehicle, AM-8123, losartan, or both. (**B** and **C**) Picrosirius red (PSR) staining of heart serial sections revealed less collagen deposition in the treated groups. (**D**) This was associated with a significant increase in EF. Data shown as individual animals (circles) and the group mean (bars) ± SEM. Data analyses were performed blinded. n = 9–10/group for histology. n = 9–14 for treated groups; n = 7 for sham for assessment of cardiac function. Significance was measured by a 1-way ANOVA with Tukey's posttest (*P < 0.05; **P < 0.01; ***P < 0.001; ****P < 0.0001).

contractility as evidenced by an increase in preload recruitable stroke work (PRSW) and the end systolic pressure-volume relationship (ESPVR) (Figure 7, C and D), both of which are load-insensitive measures of LV performance. This did not translate to a significant increase in SV, HR, or MAP relative to vehicle (Supplemental Figure 10, A–C). AM-8123 infusion resulted in a modest but significant decrease in MAP/CO, suggesting a decrease in SVR or cardiac afterload (Supplemental Figure 10D). No change in the relaxation parameters, dP/dt min and tau, were observed (Supplemental Figure 10, E and F). When hemodynamic measurements were made in conscious dogs that had tachypacing-induced HF, we did not observe significant hemodynamic improvements with AM-8123 (Supplemental Figure 11). The differential effect of AM-8123 in anesthetized versus conscious dogs may be attributed to the well-known sympatholytic effects of general anesthesia.

APJ small-molecule agonist AMG 986 is well tolerated, causing no adverse effects in nonclinical toxicology models. To support the clinical development of AMG 986, toxicology studies were conducted in accordance with regulatory guidelines. In the pivotal toxicology studies, AMG 986 was well tolerated and caused no adverse effects at oral daily doses up to 1000 and 300 mg/kg in 28-day repeat-dose toxicology studies in rats and canines, respectively. Mean plasma drug exposures (AUC) (368 and 538 μg/h/mL) and Cmax values (141 and 98 μg/mL) in the rat and canine, respectively, provide adequate multiples over the anticipated efficacious dose in humans based on an approximately 10% increase in EF in the tachypaced canine model of HF.

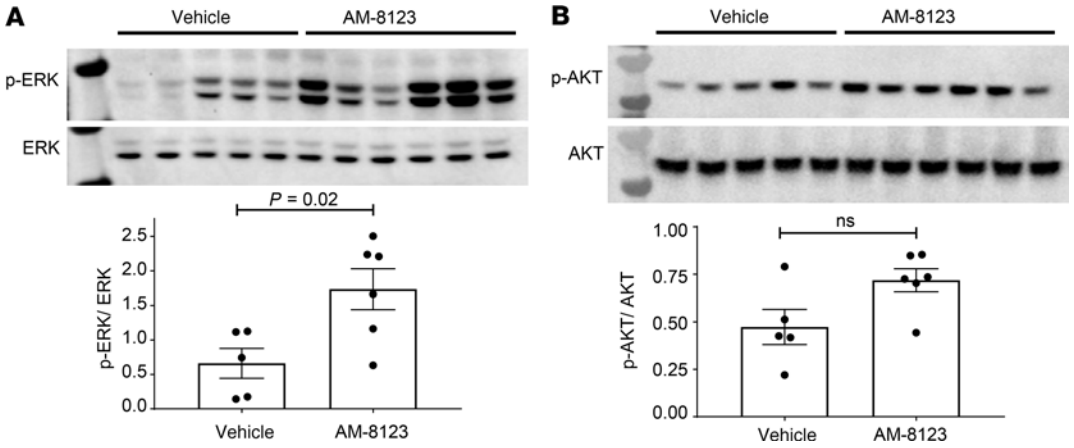

Figure 5. Chronic administration of AM-8123 induces known APJ signaling pathways. Western blots reveal an increase in (**A**) ERK and a trend toward increased (**B**) AKT phosphorylation in LV cardiac tissue collected from a subset of animals as part of the study presented within Figure 4. Individual data points (circles, *n* = 5–6) and group mean (bars) ± SEM are shown. Significance measured by a 2-tailed unpaired *t* test. See full blots in Supplemental Figures 19 and 20.

No significant changes in body weight or clinical chemistry endpoints were observed for any dose groups (Supplemental Figures 12–15). In safety pharmacology studies, AMG 986 caused no adverse effects on the central nervous or respiratory system when evaluated in rats at single doses up to 1000 mg/kg. AMG 986 did not significantly inhibit the human *ether à go go* related gene channel current in vitro (10% inhibition at 300 μM) (Supplemental Figure 16) and had no meaningful dose-dependent impact on ECG or HR when evaluated in an exploratory 28-day repeat-dose toxicity study in telemetered canines at doses up to 300 mg/kg (Supplemental Figures 17 and 18). AMG 986 was not genotoxic and did not demonstrate any significant inhibition of an extensive panel of phosphodiesterases (Supplemental Table 1). Furthermore, selectivity was accessed using the aequorin luminescence assay for a panel of 13 GPCRs. No activity was observed against any of the GPCRs evaluated (Supplemental Table 2). Additionally, AMG 986 falls within a structural class of generally potent Pgp substrates, which subsequently are not expected to cross the blood-brain barrier. Collectively, these data suggest that AMG 986 has a favorable risk-benefit profile to warrant clinical evaluation.

Discussion

HF remains a leading cause of death worldwide, and new medications are desperately needed to manage disease progression. The apelin/APJ axis is a novel pathway implicated in a variety of diseases, including HF (49–52). Given the short half-life of the endogenous peptide ligands, a key question remained related to the feasibility of developing a safe and effective small-molecule APJ agonist. Here, we demonstrate that it is feasible to develop an APJ agonist that mimics the endogenous ligand pharmacologically and is safe to proceed into clinical studies. The small-molecule agonists presented here exhibit low nanomolar potency for G protein signaling, β-arrestin recruitment, and receptor internalization. Both AM-8123 and AMG 986 were comparable to the endogenous ligand, pyr-apelin-13, in these assays, and both exhibited similar potency for G protein signaling and β-arrestin recruitment. Additionally, no discernible differences in efficacy were observed for AMG 986 and AM-8123 following acute infusion in either the rat MI or tachypaced dog models. Given the structural similarity and comparable efficacy, AM-8123 was used as a tool molecule during follow-on studies, such as the chronic MI rat study and the anesthetized versus conscious tachypaced canine study, as AMG 986 was progressing toward clinical development.

AM-8123 and AMG 986 function as balanced APJ agonists, equally potent for stimulating G protein signaling and β-arrestin recruitment. It is worth noting that G protein–selective, "biased" small molecules were also identified and evaluated through the tachypaced canine HF model. However, no clear advantage was observed for the biased molecules for any relevant cardiovascular endpoints. As such, a strategic decision was made in favor of developing unbiased agonists, given they were further along in development.

Our molecular modeling results demonstrate that AM-8123 possesses features mimicking the C-terminal part of apelin-13, especially the Met11 and Phe13 residues. This coincides with the importance of the C-terminal part of apelin-13 in receptor binding and activity revealed by previous studies (46, 53–55). For example, the alanine scanning results demonstrated that M11A mutation decreases the receptor binding (55).

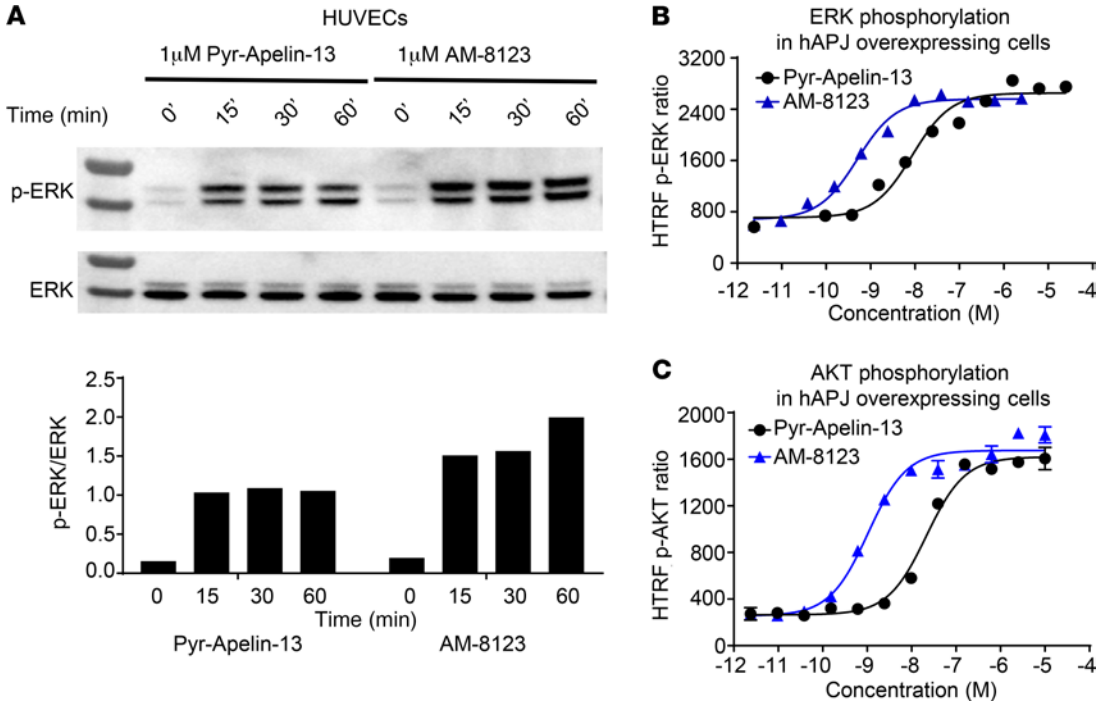

Figure 6. Second messenger signaling in response to AM-8123 and pyr-apelin-13 treatment. (**A**) Both AM-8123 and pyr-apelin-13 result in ERK phosphorylation in HUVECs grown under hypoxic conditions. Additionally, AM-8123 and pyr-apelin-13 exhibit a dose-dependent increase in both (**B**) ERK and (**C**) AKT phosphorylation in CHO cells overexpressing hAPJ. See full blots in Supplemental Figure 23. HTRF, homogeneous time resolved fluorescence.

Besserer-Offroy et al. discovered that the C-terminal Phe13 of apelin plays a key role in β-arrestin recruitment, which is in accordance with the findings of Iturrioz et al. that this residue is important for APJ internalization (53, 54). Interestingly, both studies demonstrated that Phe13 of apelin-13 does not play a major role in receptor binding, activation of $G\alpha_{i/o}$, or inhibition of cAMP production. In our study, however, AM-8123 shows activities in both β-arrestin recruitment and Gα protein activation. The latter activity may be attributed to the unique elements of AM-8123, such as its methylpyridine group that inserts deeper into the orthosteric site than apelin-13. Thus, both features mimicking the C-terminal part of apelin-13 and the unique elements make AM-8123 a potent agonist of APJ although it is smaller than the endogenous peptide ligand.

The APJ small-molecule agonists presented here alter cardiac hemodynamics in 2 rat models and 1 canine model of impaired cardiac function. Systolic function was improved in all models. Additionally, the MAP/CO ratio, which is used to approximate SVR, decreased in all models. CO is a major factor that determines MAP, where an increase in CO leads to an increase in MAP. A decrease in SVR in all models suggests that the small-molecule agonists affect vascular tone even in the absence of a sustained change in blood pressure. Finally, changes were observed in cardiac hemodynamics that were unique to the model, the duration of treatment (acute vs. chronic), or the state of the animal (conscious vs. anesthetized), which will be discussed in detail, below.

Acute IV infusion in ZSF1 obese rats improved systolic function as observed by the increase in EF and SV alone and in combination with dobutamine. This was associated with a modest but significant increase in HR in the absence of dobutamine, which could contribute to the favorable hemodynamic response. During dobutamine challenge, when HR was more similar between AMG 986– and vehicle-treated groups, a significant increase in both EF and SV was observed (Figure 3), suggesting that the improvement in cardiac performance under conditions of stress or hemodynamic challenge is, at least in part, independent of HR.

The vascular effects caused by modulation of the apelin/APJ axis are complex. Apelin can act as a potent vasodilator or vasoconstrictor, depending on the underlying state of the vascular bed (12, 56–58). APJ is expressed in both endothelial and smooth muscle cells within the vessel wall, and apelin's vasodilatory properties are driven, in part, by endothelium-derived increases in NO bioavailability (58–63). ZSF1 obese rats exhibit endothelial dysfunction (64). Thus, it remains possible that endothelial dysfunction in this model may have muted the vasodilatory effects associated with APJ activation.

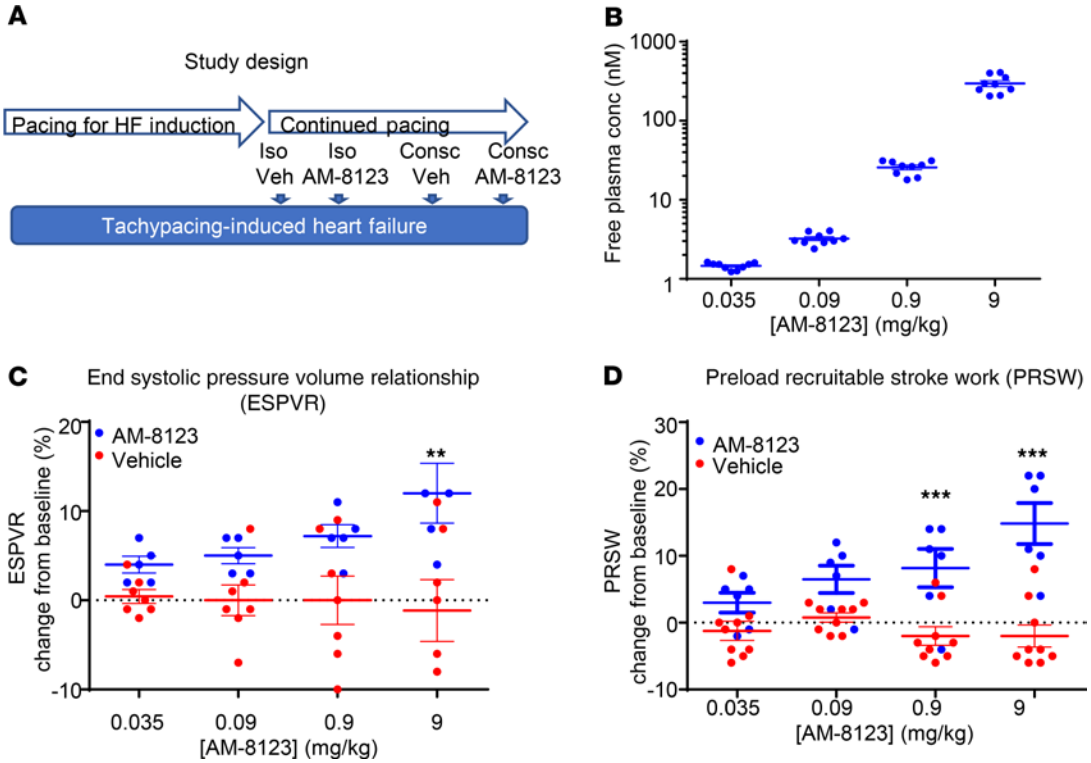

Figure 7. Acute administration of the APJ small-molecule agonist AM-8123 improves markers of cardiac function in beagles with tachypacing-induced HF under isoflurane anesthesia. (**A**) Instrumented animals were subjected to an overdrive pacing protocol for approximately 4 weeks to induce HF. Pacemakers were turned off at least 15 minutes prior to the initiation of treatment. Vehicle (Veh) and AM-8123 were administered to anesthetized (Iso) animals in a randomized manner. For AM-8123, all canines were infused with escalating doses of AM-8123, resulting in increasing levels of (**B**) exposure and a dose-dependent increase in 2 load-insensitive measures: (**C**) PRSW and (**D**) ESPVR. Individual data points (circles) and group mean (bars) ± SEM are shown. Data analyses were performed blinded. Significance measured by a 2-way ANOVA with Tukey's posttest (**$P < 0.01$; ***$P < 0.001$).

Chronic oral administration of AM-8123 did not result in cardiac hypertrophy, a form of cardiac remodeling that may facilitate transient stress adaptation but plays a more maladaptive role during chronic stress (65–68). Previous work has shown that the apelin/APJ axis can play a protective role by attenuating the development of cardiac hypertrophy under a variety of conditions. For example, stimulation of the apelin/APJ axis has been shown to alleviate angiotensin II–induced, oxidative stress–induced, as well as exercise-induced pathological hypertrophy (65). Additionally, apelin administration was found to decrease the heart weight/body weight ratio in mice post-MI (69). We believe these protective effects may have blunted cardiac hypertrophy that one would expect from the chronic administration of a traditional inotrope.

Chronic administration of AM-8123 decreased collagen levels, suggesting an attenuation of post-MI remodeling and border zone expansion. The decreased levels were associated with improved diastolic function, suggesting that the reduction in collagen content improved myocardial compliance. Previous work has shown that apelin can ameliorate myocardial damage in MI rats via enhancement of myocardial NO production and decreased lipid peroxidation (70). The apelin/APJ pathway has also been shown to promote angiogenesis (15, 71–76). Increased vascularization at the site of myocardial injury is known to reduce scar formation and preserve cardiac function (77–79). The reduction in collagen volume observed with this small-molecule agonist may be driven by these mechanisms and is supported by the trend toward increased eNOS phosphorylation in LV cardiac tissue as well as the robust increase in ERK phosphorylation in endothelial cells grown under hypoxic conditions.

There were no significant improvements in cardiac function following the coadministration of AM-8123 and losartan relative to the individual therapies. If these observations translate to the clinical setting, then this raises the possibility that an APJ agonist may add little to available low-cost RAS antagonist therapies that are widely prescribed to HF and hypertensive patients. In this instance, APJ agonism should be considered in situations where RAS antagonist therapies are intolerable, for example, in patients where adequate doses of losartan or other RAS antagonists are limited by low blood pressure or otherwise contraindicated.

Acute IV infusion of AM-8123 in anesthetized beagles with HF resulted in a dose-dependent increase in PRSW and ESPVR but not *dP/dt* max. We believe ESPVR and PRSW are better measures of cardiac contractility because they are less sensitive to load relative to *dP/dt* max. The increase in both PRSW and ESPVR under anesthesia suggests that under these conditions, AM-8123 increased myocardial contractility. These data are consistent with previous work indicating that apelin-activated APJ increases PRSW in anesthetized mice (40). Why *dP/dt* max, a load-dependent measure of contractility, was unchanged in the tachypacing-induced HF beagle model but was increased in the LAD ligation–induced MI rat model is unclear. It is known that autonomic balance is different in different species, and it is feasible that load-dependent effects are more sensitive to changes in autonomic tone balance.

No effect on cardiovascular or hemodynamic function was observed during acute IV infusion of AM-8123 in conscious tachypacing-induced HF beagles. Given that the anesthetized arm of the study was conducted in the same animal prior to the conscious arm of the study, it is possible that the small molecule desensitized APJ during administration under anesthesia. However, it is worth noting that the half-life of AM-8123 is 2.2 hours, and there was a minimum of a 7-day washout following the acute infusion of AM-8123. Therefore, 1 week after an initial exposure to AM-8123, we would anticipate there to be approximately 5×10^{-240}%, or approximately 0, remaining. We believe that this provides time for APJ to become resensitized if desensitization occurred.

General anesthesia alters sympathetic activity and can cause a cardio-depressed state, as evidenced by decreased HR, *dP/dt* max and min, as well as EF. This may result in a larger window to observe a favorable hemodynamic response. Additionally, HR is inversely proportional to EDV. As HR decreases, EDV increases in anesthetized animals, leading to an increase in passive stretch, or preload. It is therefore possible that passive stretch increases cardiomyocyte length, augmenting APJ-induced cardiac effects in a load-dependent manner.

There are several limitations with this study. Our lack of complete understanding related to the mechanism by which general anesthesia influences the acute hemodynamic effects of the APJ small-molecule agonists is one limitation. Additionally, the relative contribution of the direct versus indirect effects of the small-molecule agonists on augmenting cardiac function is another limitation. Understanding both would aid in our general understanding of APJ biology and facilitate clinical assessment. Finally, the translatability of animal models is always a concern, and it remains unclear whether the improvements in acute LV hemodynamics will predict our ability to improve cardiac function in a patient population expected to be significantly more heterogeneous than our animal cohorts.

APJ is considered an emerging therapeutic target for a variety of disease indications (49–52). We show here that it is feasible to develop a potent small-molecule agonist suitable for clinical studies. Apelin activation of APJ exhibits pleiotropic effects on the cardiovascular system (20). Our data are consistent with the pleiotropic actions of APJ and indicate that small-molecule APJ activation results in improvements in vascular tone as well as load-insensitive measures of cardiac function. Collectively, this activity results in a globally favorable hemodynamic effect, and sustained treatment leads to reduced collagen burden and improved myocardial compliance. However, the lack of additivity on top of RAS antagonist therapies raises concerns related to the utility of modulating the APJ axis for a chronic HF indication.

Methods

Small-molecule synthesis. AM-8123 and AMG 986 were prepared as described (WO2016187308A1, Triazole agonists of the APJ receptor) (43).

In vitro assays. APJ activation was measured using the scintillation proximity assay–based GPCR assay as well as the HitHunter cAMP assay (kit 90-0075-03, DiscoveRx). APJ internalization was measured using the PathHunter GPCR internalization assay (DiscoveRx), and β-arrestin recruitment was measured using the ProLink β-gal complementation technology (93-0001, DiscoveRx). A detailed description of each assay can be found within the Supplemental Methods.

For saturation binding of ^{3}H AM-8123, APJ gene mutations were generated by PCR and subcloned into the pFLAG-CMV-3 vector (MilliporeSigma). The mutant plasmids were prepared by Biozilla. Cell membranes were prepared as described previously (80) from HEK293T cells (ATCC, CRL-11268) transiently transfected with hAPJ mutants. ^{3}H AM-8123 was diluted serially with ice-cold binding buffer (20 mM HEPES at pH 7.5, 5 mM $MgCl_2$, 100 mM NaCl, and 0.1% w/v fatty acid–free BSA). The assay was performed with 5–10 μg of membrane protein in a 96-well plate incubated with the radiolabel at room temperature for 1.5 hours

with gentle agitation. Nonspecific binding was determined in the presence of 1 μM unlabeled pyr-apelin-13 or AM-8123. The binding reactions were terminated by filtration with a GF/C filter plate followed with 5 washes of ice-cold buffer. Then, 50 μL of scintillant was added to each well of the plate, and radioactivity was measured using the TopCount Microplate Scintillation counter (PerkinElmer). Saturation binding curves were generated using 3 replicates (separate experiments) for each data point.

For confocal microscopy, to generate β-arrestin 2-GFP construct, β-arrestin 2 was fused to the N-terminal of GFP and subcloned into pIREShyg3 vector. U2OS cells were transfected with pIREShyg3-arrestin-GFP plasmid with Lipofectamine LTX according to the manufacturer's protocol (Thermo Fisher Scientific). β-arrestin 2-GFP stable cells were selected with medium containing 500 μg/mL Hygromycin B from Thermo Fisher Scientific. HA-tagged, human, full-length APJ in pJiF1.1 vector was used as a template to generate APJ Bacmids by PCR-based site-directed mutagenesis. The resulting Bacmids were used to generate BacMam virus by infecting insect SF9 cells (Thermo Fisher Scientific) according to standard protocol.

U2OS cells (ATCC) stably expressing β-arrestin 2-GFP were seeded into a 6-well plate at a density of 80,000 cells/well and grown overnight. Attached cells were transduced with BacMam virus of hAPJ fused by HA tag. Six hours after virus transduction, cells were suspended and seeded at a density of 30,000 cells/well into 8-well chamber dishes and grown overnight before experiments. Cell surface receptors were stained with 10 μg/mL Alexa Fluor 594–conjugated anti-HA antibody (Invitrogen, Thermo Fisher Scientific, catalog A-21288) at room temperature for 1 hour. The cells were then stimulated with AM-8123 at final concentration of 100 nM in freshly prepared medium. The distribution of APJ and β-arrestin 2-GFP were monitored using a Leica SP8 confocal microscope.

The phospho-AKT and phospho-ERK in vitro assays quantified the ratio of phospho/total protein levels. ERK and AKT phosphorylation in CHO-hAPJ cells (generated by Amgen) were quantified using the Phosph-ERK 1/2 (Thr202/Tyr 204) kit (Cisbio, 64ERKPEG) and the Phosph-AKT (Ser473) kit (Cisbio, 64AKSPEG), respectively, according to the supplied protocols in cells seeded at 50,000 cells/well in 96-well plates.

For analysis in HUVECs (Lonza, C2519A), cells were seeded at 3 million cells in 10-cm dishes. Cells were grown under hypoxic conditions (1% O_2, 5% CO_2, and 94% N_2) for 16 hours before the addition of 1 μM pyr-apelin-13 or 1 μM AM-8123 and incubated for 15, 30, or 60 minutes and compared to untreated control cells. Cells were subsequently washed and scraped into individual falcon tubes, centrifuged to remove the supernatant, and resuspended in RIPA buffer (Cell Signaling Technology, 9806) containing 1X Halt protease and phosphatase inhibitor cocktail (Thermo Fisher Scientific, 1861281). Western blot analyses were conducted with 100 μg of total protein/lane using a NuPAGE 4-12% Bis-Tris Gel (Thermo Fisher Scientific) run at 100 V. Samples were then transferred using the iBlot gel transfer system (Life Technologies, Thermo Fisher Scientific), and phospho- and total ERK were detected using antibodies from Cell Signaling Technology (4370 and 9107) at 1:500 dilution.

For Western blot analysis of LV cardiac tissue, protein was isolated from flash-frozen samples using T-PER tissue protein Extraction Reagent (Thermo Fisher Scientific, 78510). Western blots were performed as described above using the following antibodies: eNOS (phospho-eNOS, pS1177, BD Transduction Laboratories, 612393, 1:500, and total eNOS, Pierce, Thermo Fisher Scientific, PA1-037, 1:500), ERK (phospho-ERK, p44/42, Cell Signaling Technology, 4370, 1:500, and total ERK, Cell Signaling Technology, 9107, 1:500), AKT (phospho-Akt, Ser473, Cell Signaling Technology, 9271, 1:1000, and total AKT, Cell Signaling Technology, 4691, 1:1000), AMPK (phospho-AMPK, Thr172, Cell Signaling Technology, 50081, 1:500, and total AMPK, Cell Signaling Technology, 2532, 1:1000).

For quantitative real-time PCR of LV cardiac tissue, RNA was isolated from flash-frozen samples using RNeasy Mini Kit (QIAGEN, 74104) and the supplied product protocol. PCR was performed using the TaqMan RNA-to-C_T *1-Step* Kit (Thermo Fisher Scientific, 4392653) according to the supplied product protocol with the following primers/probes: Col1A1 (Rn01463848_m1), Tgfb1 (Rn00572010_m1), Acat2 (Rn01526241_g1), Postn (Rn01494627_m1), and Gapdh (Rn01775763_g1).

Molecular modeling. The PPM server was used to calculate rotational and translational positions of APJ in a membrane (81). A 2-step minimization was further performed with Prime in Schrödinger considering implicit membrane environment: first, only AP-13 and residues within 5 Å of it were minimized; then the whole complex was minimized.

For the APJ/AM-8123 complex model, the initial model of WT APJ (residues 26–327) was built via homology modeling in Discovery Studio, with the cocrystal structure of APJ and a small-molecule

agonist (AM-8123's analog, our unpublished data) as the template. The ICL3 loop region was optimized with Prime Refine Loops in Schrödinger, with implicit membrane placed as aligned APJ structure (PDB ID 5VBL) from the Orientations of Proteins in Membranes database (81). The APJ model was validated with "Verify Protein (Profiles-3D)" in Discovery Studio. The Verify Score of the model is 158.64, which is higher than the Verify Expected High Score 137.429 and indicates the model has high quality. Then the APJ model was used for molecular docking of AM-8123 with Glide (XP mode) in Schrödinger (Schrödinger Release 2017-3). Finally, the restrained minimization was applied to the top-ranked binding pose together with APJ to generate the APJ/AM-8123 complex model.

Study approval. All animals were housed at AAALAC International–accredited facilities, and all research protocols were approved by their respective Institutional Animal Care and Use Committees (Amgen and QTest Labs, Columbus, Ohio, USA). The pivotal nonclinical safety studies were performed in accordance with International Council for Harmonisation of Technical Requirements for Pharmaceuticals for Human Use M3 and Good Laboratory Practices (United States Code of Federal Regulations, Title 21, Part 58: Good Laboratory Practice for Nonclinical Laboratory Studies). A detailed description of the in vivo work can be found within the Supplemental Methods.

Statistics. In vitro dose-response curves were analyzed using Genedata Screener. Raw data were normalized to DMSO. Pyr-apelin-13 was used as a positive control. The curve-fitting algorithm used for dose response data analysis in Genedata Screener is a custom implementation of the robust regression with outlier detection curve-fitting algorithm, which uses a 4-parameter logistical (4PL) Hill model. The in vitro results were expressed as the mean ± SEM. Results were considered significantly different for $P < 0.05$. The statistical test used for each experiment is indicated within the figure legend. A 2-tailed *t* test was used for experiments with 2 groups without repeated measurements. A 1-way ANOVA was used for experiments with 3 or more groups. A 2-way ANOVA was used for experiments with 2 or more groups with repeated measurements. All the in vivo results were expressed as the mean ± SEM.

Author contributions

BA, YC, QG, KMH, RWC, MF, LAH, JH, J Wang, PD, VP, GS, AYK, DL, KN, YQ, BG, VC, and JC conceptualized and designed experiments. QG, PD, VP, and GS generated small molecules or reagents. BA, YC, QG, WS, RC, YZ, SM, XM, XL, YS, J Wong, NL, AB, JT, LAH, JM, VP, J Wang, GS, DL, KN, YQ, BG, VC, and JC conducted experiments. BA, YC, KMH, RWC, MF, RC, LAH, HMV, GS, AYK, SR, and MMV aided in drafting the manuscript. BA, YC, QG, and KMH share co–first authorship based on their equal but distinct contributions. The coauthorship order was determined based on involvement with putting together this manuscript.

Acknowledgments

We thank Julie Freebersyser, Cheryl Loughery, Maya Patrick, Josh Dobroff, Alysha Hoffman, Jackson Khin, and Danny Wong for technical assistance; Wen-Chen Yeh for helpful discussions; Jason Legg for feedback related to the statistical tests used to measure significance; and Jeff Reagan, Bill Richards, and Saptarsi Halder for critical review of the manuscript. All research was funded by Amgen, Inc.

Address correspondence to: Brandon Ason, Amgen, Inc, 1120 Veterans Blvd., South San Francisco, California 94080, USA. Phone: 650.244.2042; Email: bason@amgen.com.

1. Gomez-Soto FM, et al. Incidence and mortality of heart failure: a community-based study. *Int J Cardiol*. 2011;151(1):40–45.
2. Tanai E, Frantz S. Pathophysiology of heart failure. *Compr Physiol*. 2015;6(1):187–214.
3. Ponikowski P, et al. 2016 ESC Guidelines for the diagnosis and treatment of acute and chronic heart failure: the Task Force for the diagnosis and treatment of acute and chronic heart failure of the European Society of Cardiology (ESC): developed with the special contribution of the Heart Failure Association (HFA) of the ESC. *Eur Heart J*. 2016;37(27):2129–2200.
4. Rogers C, Bush N. Heart failure: pathophysiology, diagnosis, medical treatment guidelines, and nursing management. *Nurs Clin North Am*. 2015;50(4):787–799.
5. Metra M, Teerlink JR. Heart failure. *Lancet*. 2017;390(10106):1981–1995.
6. Mozaffarian D, et al. Heart Disease and Stroke Statistics-2016 Update: a report from the American Heart Association. *Circulation*. 2016;133(4):e38–360.
7. Dwyer-Lindgren L, et al. US County-Level Trends in Mortality Rates for Major Causes of Death, 1980-2014. *JAMA*. 2016;316(22):2385–2401.
8. O'Dowd BF, et al. A human gene that shows identity with the gene encoding the angiotensin receptor is located on chromo-

some 11. *Gene*. 1993;136(1-2):355–360.
9. Chen MM, et al. Novel role for the potent endogenous inotrope apelin in human cardiac dysfunction. *Circulation*. 2003;108(12):1432–1439.
10. Kleinz MJ, Davenport AP. Immunocytochemical localization of the endogenous vasoactive peptide apelin to human vascular and endocardial endothelial cells. *Regul Pept*. 2004;118(3):119–125.
11. Sheikh AY, et al. In vivo genetic profiling and cellular localization of apelin reveals a hypoxia-sensitive, endothelial-centered pathway activated in ischemic heart failure. *Am J Physiol Heart Circ Physiol*. 2008;294(1):H88–H98.
12. Maguire JJ, Kleinz MJ, Pitkin SL, Davenport AP. [Pyr1]apelin-13 identified as the predominant apelin isoform in the human heart: vasoactive mechanisms and inotropic action in disease. *Hypertension*. 2009;54(3):598–604.
13. Lv SY, Yang YJ, Chen Q. Regulation of feeding behavior, gastrointestinal function and fluid homeostasis by apelin. *Peptides*. 2013;44:87–92.
14. Melgar-Lesmes P, et al. Hypoxia and proinflammatory factors upregulate apelin receptor expression in human stellate cells and hepatocytes. *Gut*. 2011;60(10):1404–1411.
15. Eyries M, et al. Hypoxia-induced apelin expression regulates endothelial cell proliferation and regenerative angiogenesis. *Circ Res*. 2008;103(4):432–440.
16. Ronkainen VP, et al. Hypoxia inducible factor regulates the cardiac expression and secretion of apelin. *FASEB J*. 2007;21(8):1821–1830.
17. O'Carroll AM, Lolait SJ. Regulation of rat APJ receptor messenger ribonucleic acid expression in magnocellular neurones of the paraventricular and supraopric nuclei by osmotic stimuli. *J Neuroendocrinol*. 2003;15(7):661–666.
18. Zhong JC, et al. The novel peptide apelin regulates intrarenal artery tone in diabetic mice. *Regul Pept*. 2007;144(1-3):109–114.
19. Llorens-Cortes C, Moos F. Opposite potentiality of hypothalamic coexpressed neuropeptides, apelin and vasopressin in maintaining body-fluid homeostasis. *Prog Brain Res*. 2008;170:559–570.
20. Barnes G, Japp AG, Newby DE. Translational promise of the apelin--APJ system. *Heart*. 2010;96(13):1011–1016.
21. Ashley E, Chun HJ, Quertermous T. Opposing cardiovascular roles for the angiotensin and apelin signaling pathways. *J Mol Cell Cardiol*. 2006;41(5):778–781.
22. Chun HJ, et al. Apelin signaling antagonizes Ang II effects in mouse models of atherosclerosis. *J Clin Invest*. 2008;118(10):3343–3354.
23. Fukushima H, Kobayashi N, Takeshima H, Koguchi W, Ishimitsu T. Effects of olmesartan on Apelin/APJ and Akt/endothelial nitric oxide synthase pathway in Dahl rats with end-stage heart failure. *J Cardiovasc Pharmacol*. 2010;55(1):83–88.
24. Siddiquee K, Hampton J, McAnally D, May L, Smith L. The apelin receptor inhibits the angiotensin II type 1 receptor via allosteric trans-inhibition. *Br J Pharmacol*. 2013;168(5):1104–1117.
25. Charles CJ. Putative role for apelin in pressure/volume homeostasis and cardiovascular disease. *Cardiovasc Hematol Agents Med Chem*. 2007;5(1):1–10.
26. Iwanaga Y, Kihara Y, Takenaka H, Kita T. Down-regulation of cardiac apelin system in hypertrophied and failing hearts: possible role of angiotensin II-angiotensin type 1 receptor system. *J Mol Cell Cardiol*. 2006;41(5):798–806.
27. Földes G, et al. Circulating and cardiac levels of apelin, the novel ligand of the orphan receptor APJ, in patients with heart failure. *Biochem Biophys Res Commun*. 2003;308(3):480–485.
28. Pitkin SL, Maguire JJ, Kuc RE, Davenport AP. Modulation of the apelin/APJ system in heart failure and atherosclerosis in man. *Br J Pharmacol*. 2010;160(7):1785–1795.
29. Atluri P, et al. Ischemic heart failure enhances endogenous myocardial apelin and APJ receptor expression. *Cell Mol Biol Lett*. 2007;12(1):127–138.
30. Tatemoto K, et al. Isolation and characterization of a novel endogenous peptide ligand for the human APJ receptor. *Biochem Biophys Res Commun*. 1998;251(2):471–476.
31. Yang P, et al. Elabela/Toddler is an endogenous agonist of the apelin APJ receptor in the adult cardiovascular system, and exogenous administration of the peptide compensates for the downregulation of its expression in pulmonary arterial hypertension. *Circulation*. 2017;135(12):1160–1173.
32. Simpkin JC, Yellon DM, Davidson SM, Lim SY, Wynne AM, Smith CC. Apelin-13 and apelin-36 exhibit direct cardioprotective activity against ischemia-reperfusion injury. *Basic Res Cardiol*. 2007;102(6):518–528.
33. Lee DK, et al. Characterization of apelin, the ligand for the APJ receptor. *J Neurochem*. 2000;74(1):34–41.
34. Chng SC, Ho L, Tian J, Reversade B. ELABELA: a hormone essential for heart development signals via the apelin receptor. *Dev Cell*. 2013;27(6):672–680.
35. Jia YX, et al. Apelin protects myocardial injury induced by isoproterenol in rats. *Regul Pept*. 2006;133(1-3):147–154.
36. Koguchi W, Kobayashi N, Takeshima H, Ishikawa M, Sugiyama F, Ishimitsu T. Cardioprotective effect of apelin-13 on cardiac performance and remodeling in end-stage heart failure. *Circ J*. 2012;76(1):137–144.
37. Sato T, et al. ELABELA-APJ axis protects from pressure overload heart failure and angiotensin II-induced cardiac damage. *Cardiovasc Res*. 2017;113(7):760–769.
38. Kleinz MJ, Baxter GF. Apelin reduces myocardial reperfusion injury independently of PI3K/Akt and P70S6 kinase. *Regul Pept*. 2008;146(1-3):271–277.
39. Rai R, et al. Downregulation of the apelinergic axis accelerates aging, whereas its systemic restoration improves the mammalian healthspan. *Cell Rep*. 2017;21(6):1471–1480.
40. Ashley EA, et al. The endogenous peptide apelin potently improves cardiac contractility and reduces cardiac loading in vivo. *Cardiovasc Res*. 2005;65(1):73–82.
41. Japp AG, et al. Acute cardiovascular effects of apelin in humans: potential role in patients with chronic heart failure. *Circulation*. 2010;121(16):1818–1827.
42. Barnes GD, et al. Sustained cardiovascular actions of APJ agonism during renin-angiotensin system activation and in patients with heart failure. *Circ Heart Fail*. 2013;6(3):482–491.
43. Chen N, et al, inventors; Amgen Inc, assignee. Triazole agonists of the APJ receptor. US patent WO2016187308A1. November 24, 2016.
44. Scimia MC, et al. APJ acts as a dual receptor in cardiac hypertrophy. *Nature*. 2012;488(7411):394–398.
45. Chen X, Bai B, Tian Y, Du H, Chen J. Identification of serine 348 on the apelin receptor as a novel regulatory phosphorylation

site in apelin-13-induced G protein-independent biased signaling. *J Biol Chem*. 2014;289(45):31173–31187.
46. Ma Y, et al. Structural basis for apelin control of the human apelin receptor. *Structure*. 2017;25(6):858–866.e4.
47. Buttrick P, Perla C, Malhotra A, Geenen D, Lahorra M, Scheuer J. Effects of chronic dobutamine on cardiac mechanics and biochemistry after myocardial infarction in rats. *Am J Physiol*. 1991;260(2 pt 2):H473–H479.
48. Anderson M, Moore D, Larson D. Comparison of isoproterenol and dobutamine in the induction of cardiac hypertrophy and fibrosis. *Perfusion*. 2008;23(4):231–235.
49. Zhou Q, Chen L, Tang M, Guo Y, Li L. Apelin/APJ system: A novel promising target for anti-aging intervention. *Clin Chim Acta*. 2018;487:233–240.
50. Wysocka MB, Pietraszek-Gremplewicz K, Nowak D. The role of apelin in cardiovascular diseases, obesity and cancer. *Front Physiol*. 2018;9:557.
51. Masoumi J, et al. Apelin, a promising target for Alzheimer disease prevention and treatment. *Neuropeptides*. 2018;70:76–86.
52. Lv SY, Cui B, Chen WD, Wang YD. Apelin/APJ system: A key therapeutic target for liver disease. *Oncotarget*. 2017;8(67):112145–112151.
53. Iturrioz X, Gerbier R, Leroux V, Alvear-Perez R, Maigret B, Llorens-Cortes C. By interacting with the C-terminal Phe of apelin, Phe255 and Trp259 in helix VI of the apelin receptor are critical for internalization. *J Biol Chem*. 2010;285(42):32627–32637.
54. Besserer-Offroy É, et al. The hypotensive effect of activated apelin receptor is correlated with β-arrestin recruitment. *Pharmacol Res*. 2018;131:7–16.
55. Fan X, et al. Structural and functional study of the apelin-13 peptide, an endogenous ligand of the HIV-1 coreceptor, APJ. *Biochemistry*. 2003;42(34):10163–10168.
56. Nagano K, Ishida J, Unno M, Matsukura T, Fukamizu A. Apelin elevates blood pressure in ICR mice with L-NAME-induced endothelial dysfunction. *Mol Med Rep*. 2013;7(5):1371–1375.
57. Mughal A, O'Rourke ST. Vascular effects of apelin: Mechanisms and therapeutic potential. *Pharmacol Ther*. 2018;190:139–147.
58. Salcedo A, et al. Apelin effects in human splanchnic arteries. Role of nitric oxide and prostanoids. *Regul Pept*. 2007;144(1–3):50–55.
59. Zhong JC, Yu XY, Huang Y, Yung LM, Lau CW, Lin SG. Apelin modulates aortic vascular tone via endothelial nitric oxide synthase phosphorylation pathway in diabetic mice. *Cardiovasc Res*. 2007;74(3):388–395.
60. Tatemoto K, et al. The novel peptide apelin lowers blood pressure via a nitric oxide-dependent mechanism. *Regul Pept*. 2001;99(2-3):87–92.
61. Japp AG, et al. Vascular effects of apelin in vivo in man. *J Am Coll Cardiol*. 2008;52(11):908–913.
62. Jia YX, et al. Apelin activates L-arginine/nitric oxide synthase/nitric oxide pathway in rat aortas. *Peptides*. 2007;28(10):2023–2029.
63. Mughal A, Sun C, O'Rourke ST. Activation of large conductance, calcium-activated potassium channels by nitric oxide mediates apelin-induced relaxation of isolated rat coronary arteries. *J Pharmacol Exp Ther*. 2018;366(2):265–273.
64. van Dijk CG, et al. Distinct endothelial cell responses in the heart and kidney microvasculature characterize the progression of heart failure with preserved ejection fraction in the obese ZSF1 rat with cardiorenal metabolic syndrome. *Circ Heart Fail*. 2016;9(4):e002760.
65. Foussal C, et al. Activation of catalase by apelin prevents oxidative stress-linked cardiac hypertrophy. *FEBS Lett*. 2010;584(11):2363–2370.
66. Wu S, et al. Activation of AP-1 through reactive oxygen species by angiotensin II in rat cardiomyocytes. *Free Radic Biol Med*. 2005;39(12):1601–1610.
67. Higuchi Y, et al. Involvement of reactive oxygen species-mediated NF-kappa B activation in TNF-alpha-induced cardiomyocyte hypertrophy. *J Mol Cell Cardiol*. 2002;34(2):233–240.
68. Xu FP, et al. Leptin induces hypertrophy via endothelin-1-reactive oxygen species pathway in cultured neonatal rat cardiomyocytes. *Circulation*. 2004;110(10):1269–1275.
69. Li L, Zeng H, Chen JX. Apelin-13 increases myocardial progenitor cells and improves repair postmyocardial infarction. *Am J Physiol Heart Circ Physiol*. 2012;303(5):H605–H618.
70. Azizi Y, et al. Post-infarct treatment with [Pyr(1)]apelin-13 improves myocardial function by increasing neovascularization and overexpression of angiogenic growth factors in rats. *Eur J Pharmacol*. 2015;761:101–108.
71. Kidoya H, et al. The apelin/APJ system induces maturation of the tumor vasculature and improves the efficiency of immune therapy. *Oncogene*. 2012;31(27):3254–3264.
72. Saint-Geniez M, Masri B, Malecaze F, Knibiehler B, Audigier Y. Expression of the murine msr/apj receptor and its ligand apelin is upregulated during formation of the retinal vessels. *Mech Dev*. 2002;110(1-2):183–186.
73. Cox CM, D'Agostino SL, Miller MK, Heimark RL, Krieg PA. Apelin, the ligand for the endothelial G-protein-coupled receptor, APJ, is a potent angiogenic factor required for normal vascular development of the frog embryo. *Dev Biol*. 2006;296(1):177–189.
74. Kasai A, et al. Retardation of retinal vascular development in apelin-deficient mice. *Arterioscler Thromb Vasc Biol*. 2008;28(10):1717–1722.
75. Kidoya H, Naito H, Takakura N. Apelin induces enlarged and nonleaky blood vessels for functional recovery from ischemia. *Blood*. 2010;115(15):3166–3174.
76. Chen D, Lee J, Gu X, Wei L, Yu SP. Intranasal delivery of apelin-13 is neuroprotective and promotes angiogenesis after ischemic stroke in mice. *ASN Neuro*. 2015;7(5):1759091415605114.
77. Smart N, et al. Thymosin beta4 induces adult epicardial progenitor mobilization and neovascularization. *Nature*. 2007;445(7124):177–182.
78. Lopez JJ, et al. Basic fibroblast growth factor in a porcine model of chronic myocardial ischemia: a comparison of angiographic, echocardiographic and coronary flow parameters. *J Pharmacol Exp Ther*. 1997;282(1):385–390.
79. Harada K, et al. Basic fibroblast growth factor improves myocardial function in chronically ischemic porcine hearts. *J Clin Invest*. 1994;94(2):623–630.
80. Swaminath G, Steenhuis J, Kobilka B, Lee TW. Allosteric modulation of beta2-adrenergic receptor by Zn(2+). *Mol Pharmacol*. 2002;61(1):65–72.
81. Lomize MA, Pogozheva ID, Joo H, Mosberg HI, Lomize AL. OPM database and PPM web server: resources for positioning of proteins in membranes. *Nucleic Acids Res*. 2012;40(Database issue):D370–D376.